processes

MDPI

*Article*

# The Whole-Aperture Pore Structure Characteristics and Their Controlling Factors of the Dawuba Formation Shale in Western Guizhou

**Kun Yuan [1,2], Wenhui Huang [1], Xianglin Chen [2], Qian Cao [3], Xinxin Fang [4,*], Tuo Lin [2,*], Chunshuang Jin [2], Shizhen Li [2], Chao Wang [2] and Ting Wang [2]**

[1] School of Energy Resources, China University of Geosciences, Beijing 100083, China; kunyuanogscgs@sina.com (K.Y.); huangwh@cugb.edu.cn (W.H.)
[2] Oil and Gas Resources Survey, China Geological Survey, Beijing 100083, China; chenxianglin2022@163.com (X.C.); jincs2002@163.com (C.J.); lishz2006@sina.com (S.L.); wangchaopku@126.com (C.W.); wangting@mail.cgs.gov.cn (T.W.)
[3] Sichuan Keyuan Testing Center of Engineering Technology, Chengdu 610091, China; cissiy0923@163.com
[4] Institute of Geomechanics, Chinese Academy of Geological Sciences, Beijing 100081, China
* Correspondence: freestarxin@163.com (X.F.); everdeer@163.com (T.L.)

**Abstract:** Since shale gas mainly occurs in shale pores, research on pore structure characteristics is the key to understanding the shale gas accumulation mechanism. The pore structure of the Lower Carboniferous Dawuba Formation shale in the Qianxi area, represented by the well QSD-1, which obtains a daily shale gas flow of 10,000 $m^3$ and represents an important breakthrough in the investigation of marine shale gas in the Upper Paleozoic region of southern China, is characterized by high-pressure mercury compression experiments and low-temperature gas adsorption ($N_2$ and $CO_2$) experiments with whole pore size. The main controlling factors affecting the pore development of the shale are discussed. (i) The micropores and mesopores are more developed in the shale, and the macropores are the second most developed in the shales of the Dawuba Formation in the Qianxi area, among which the mesopores and macropores contribute most to the pore volume and the micropores and mesopores contribute most to the pore-specific surface area. (ii) The microfractures and interlayer pores of clay minerals are developed in the shales of the Dawuba Formation, which are the main storage spaces for hydrocarbon gases. (iii) The main factors affecting the adsorption capacity of the shales of the Dawuba Formation in the Qianxi area are the organic carbon content and clay mineral content of the shales, both of which have an obvious positive correlation with the variation of pore structure.

**Keywords:** taphrogenic trough; Qianshuidi 1 well; carboniferous strata; pore structure; total pore volume



**Citation:** Yuan, K.; Huang, W.; Chen, X.; Cao, Q.; Fang, X.; Lin, T.; Jin, C.; Li, S.; Wang, C.; Wang, T. The Whole-Aperture Pore Structure Characteristics and Their Controlling Factors of the Dawuba Formation Shale in Western Guizhou. *Processes* **2022**, *10*, 622. https://doi.org/10.3390/pr10040622

Academic Editor: Carlos Sierra Fernández

Received: 9 February 2022
Accepted: 18 March 2022
Published: 22 March 2022



## 1. Introduction

Since the "shale gas revolution", China has carried out a lot of exploration work on shale gas resources [1–9]. However, there are few breakthroughs in Carboniferous strata in South China with great oil and gas potential [10–14], and there are few studies on the pore development and its main controlling factors of Carboniferous shale [13,14]. In 2021, well QSD-1 was deployed in the Liupanshui area of Qianxi, which was tested in the Carboniferous Dawuba Formation and obtained 10,000 $m^3$/D shale gas flow, achieving a major breakthrough in the investigation of shale gas in the Lower Carboniferous area of South China. Drilling revealed that the shale thickness of the Dawuba Formation was nearly a kilometer, and 53 sets of gas reservoirs were comprehensively interpreted, with the highest total hydrocarbon value of 63.4%. As an example of typical shale gas drilling in the area, this paper takes the core samples from the Dawuba Formation in Well QSD-1 as the research object, characterizes the whole pore size of the shale pore structure, and

discusses its influencing factors, in order to provide reference for shale gas investigation in the Qianxi area.

Shale gas occurs mainly as free gas in pores and natural fractures, adsorbed gas in organic matter and clay minerals, dissolved gas in residual oil, and in water in shale reservoirs [15,16]. The size, volume, shape, connectivity and permeability of the pores significantly influence shale gas enrichment and exploration [17]. The pore structure and fracture systems have been characterized by researchers based on various models [18–20]. For example, the low temperature $CO_2$ and $N_2$ adsorption are widely used to characterize the pore distributions of micropores (<2 nm) and mesopore size (2–50 nm), respectively. The high-pressure mercury injection method is used to characterize the pore distributions of macropores (>50 nm).

The shale characteristics of the Lower Paleozoic Silurian strata represented by the Sichuan Basin have been extensively studied [21]. In contrast, due to the large difference in mineral composition and strong heterogeneity of shale in the Upper Paleozoic marine rocks in southern China, the pore structure characteristics and their main controlling factors are quite different from those in the Lower Paleozoic strata [22].

In order to understand the pore structure characteristics of shale in the Dawuba Formation in Qianxi area and to understand the enrichment mechanism of shale gas in the Lower Carboniferous, qualitative and quantitative studies of the shale in the Dawuba Formation were carried out by FE-SEM, low temperature gas adsorption ($N_2$ and $CO_2$) and high-pressure mercury injection. The pore structure of the shale in the Dawuba Formation was characterized from different scales. The pore structure parameters such as specific surface area, pore size distribution and pore volume of the shale were obtained, and the main controlling factors were analyzed.

## 2. Experimental Scheme and Sample Selection

### *2.1. Sample Selection*

The shale samples selected in this paper were taken from the cores of different layers of the Dawuba Formation in Well QSD-1, which was located in the Qiannan depression, southwestern China (Figure 1). The study area is located in the west part of the Qiannan depression, and confined by the Ziyun and Guiyang fault. Under the tectonic processes of multiple stresses, the Carboniferous, Permian and Triassic strata have undergone strong structural deformation and denudation of different extents. In the Indosinian-Yanshan and Himalayan stages, strong folds and thrust nappes resulted in massive shortening deformation.

According to the lithology and electrical characteristics, and combined with the outcrop situation of the surrounding strata, the shale samples can be divided into four sections from bottom to top [23,24]. (1). The first member of the Dawuba Formation is the thickest and most uniform lithology member of this formation, which is mainly composed of thick black mudstone. (2). The shale in the second member of the Dawuba Formation is thin interbedded sandwiched in marl, and the shale lamellation is well developed. (3). The third member of the Dawuba Formation is grayish-black calcareous shale, mudstone, and dark gray argillaceous limestone mixed with grayish-black carbonaceous mudstone, and the interbedded structure of calcareous mudstone and micritic limestone is developed. (4). The fourth member of the Dawuba Formation is characterized by dark gray and grayish-black marl with carbonaceous shale and calcareous mudstone (Figure 2).

In order to ensure the distinguishability of the samples, nine samples from different members of the Dawuba Formation were selected for the high-pressure mercury injection experiment and the low-temperature gas adsorption experiment. At the same time, the organic carbon content, maturity, mineral composition and rock density of the samples were tested (Table 1) in order to fully reflect the pore structure characteristics of Dawuba Formation shale.

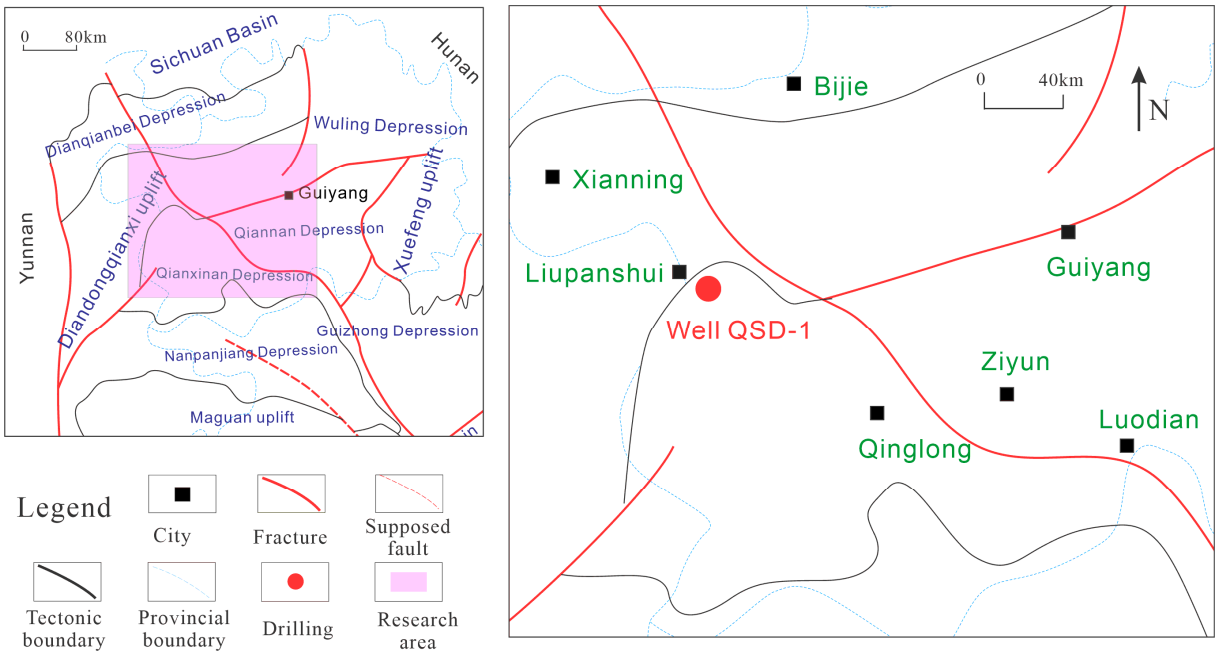


**Figure 1.** Study area and well location of Qianshuidi 1.

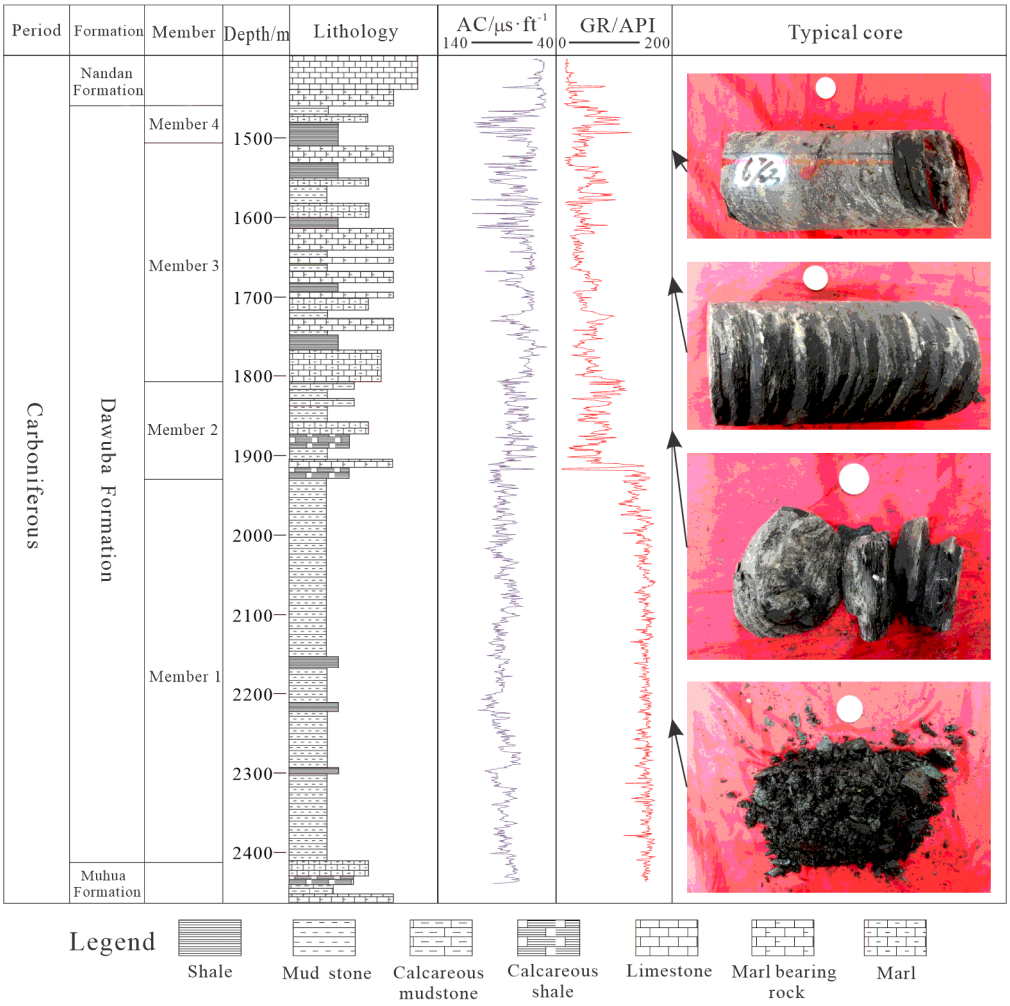


**Figure 2.** Stratigraphic characteristics and division scheme of the Dawuba Formation in Well QSD-1.

**Table 1.** Shale sample parameters of the Dawuba Formation in the Qianxi area.

| Group | Member | Depth/m | TOC/% | Ro/% | Main Mineral Component Content/% | | | | | Rock Density/g·cm$^3$ |
|---|---|---|---|---|---|---|---|---|---|---|
| | | | | | Quartz | Calcite | Dolomite | Pyrite | Clay Mineral | |
| Dawuba Formation | Member 4 | 1648.10 | 0.76 | 2.17 | 12 | 76 | 3 | 1 | 5 | 2.65 |
| | Member 3 | 1649.95 | 0.7 | 2.28 | 5 | 83 | 2 | 1 | 7 | 2.66 |
| | | 1656.50 | 0.53 | 2.18 | 9 | 74 | 7 | 1 | 9 | 2.66 |
| | | 1660.20 | 0.58 | 1.95 | 10 | 56 | 19 | 2 | 13 | 2.67 |
| | | 1682.25 | 0.99 | 2.32 | 16 | 37 | 30 | 2 | 15 | 2.40 |
| | | 1687.40 | 0.96 | 2.19 | 19 | 27 | 31 | 2 | 21 | 1.78 |
| | | 1695.59 | 0.88 | 2.18 | 12 | 34 | 33 | 1 | 20 | 2.21 |
| | Member 2 | 1931.25 | 1.08 | 2.29 | 8 | 12 | 37 | 3 | 40 | 2.69 |
| | Member 1 | 1940.90 | 1.22 | 2.57 | 27 | 0 | 4 | 0 | 69 | 2.49 |

### 2.2. Mineral Composition Analysis

A commonly used and statistically valid method to evaluate minerals in shale reservoirs is X-ray diffraction. The diffract grams were recorded in detail from 4° to 70° at a scanning speed of 1° 2θ/min by a Rigaku automated powder diffractometer (D/MAX-RA) equipped with a Cu X-ray source (40 Kv, 35 mA). The samples from the Dawuba shale were analyzed for whole-bulk and clay fraction mineralogy by quantitative X-ray diffraction following two independent processes. First, the bulk mineral composition of the powder sample was determined at this stage to only include the total clay content. The whole-rock samples were analyzed over an angular range of 4° to 70° 2θ at a scanning speed of 1° 2θ/min. Second, the individual clay mineral content of the clay fractions separated from the rock powder sample was determined. The clay minerals were analyzed over an angular range of 3° to 65° 2θ at a scanning speed of 1.5° 2θ/min. The quantification of the minerals was based on calculations of the integrated area using JADE 5 software.

### 2.3. SEM Observation

A ZEISS Sigma 300 (Oberkochen, Germany) SEM and Bruker Quantax 200G (Berlin, Germany) spectrometer were used to visualize the shale minerals and micropores of the Dawuba Formation. The organic matter, porosity, fracture distribution, size and pore connectivity were quantitatively described [25]. The porosity of the dry samples was determined from the grain density obtained from helium pycnometry (skeletal density) and the bulk volume of the plugs was calculated from mercury immersion (bulk density). The total porosity was calculated from the difference between the bulk and skeletal densities. A Gatan model 685.C (Pleasanton, CA, USA) was used for argon ion polishing in the SEM observations. Ar ion polishing is a common processing procedure carried out before observing under SEM. The samples were milled through a two-step process: (1) source operated at 2.5 kV for 2 h, followed by (2) source operated at 1.0 kV for 1 h. Each ion milling step used a 40% focus and 5° tilt angle, and the samples were continuously rotated 360° to ensure the entire surface was milled and common induced features such as curtaining were minimized.

### 2.4. High-Pressure Mercury Injection Experiment

A high-pressure mercury injection experiment is mainly used to analyze the macropore development in shale. The AutoPore 9500 mercury injection instrument from Micrometrics Instrument Co., Ltd. (Shanghai, China) is used for testing and analysis. The maximum external pressure is 400 MPa (60,000 psia). The experimental steps are based on the national standard. Before the test, the cylindrical samples (diameter 2.5 cm, length 3 cm) were first dried (dried at 150° or higher temperature for an hour), and mercury was injected into the sample tube under vacuum conditions. The test analysis was carried out at low-pressure and high-pressure stages, respectively. During the low-pressure test, the pressure was increased incrementally. When the maximum external pressure was reached, the pressure was reduced to atmospheric pressure, and the sample tube was moved into the high-pressure station for analysis. At the same time, mercury was filled into the dilatometer under vacuum conditions. The continuous pressure gradually increased the mercury to fill the pores, so as to obtain the relationship curve between the press-in amount and the pressure [26,27]. The distribution of the pore structure characteristic parameters of the different samples could then be obtained by analysis. To minimize the potential effects of the formation of artificially induced microfractures in the cylindrical sample processing, samples without any microfractures on the surface were used. However, it is hard to be certain that no artificially induced microfractures occurred in these samples.

### 2.5. Low-Temperature $N_2$ and $CO_2$ Adsorption Experiments

$N_2$ and $CO_2$ were selected as the adsorbed gas, and the isothermal adsorption curve was obtained by measuring the adsorption capacity of the sample under different pressures. The distribution of the pore structure characteristic parameters such as the pore size, specific

surface area and pore volume of the sample was calculated by BET and BJH models [27]. Among them, the liquid nitrogen adsorption–desorption test was used to characterize the mesoporous distribution characteristics of the sample. The instrument was an ASAP 2460 automatic specific surface and pore size analyzer. The relative pressure range of the isothermal adsorption–desorption experiment of the instrument is 0.00–0.995. The pore size range that can be tested is 0.35 nm–400 nm, and the minimum specific surface area that can be tested is 0.0005 $m^2/g$.

The samples were ground to powder with the particle size of 60–80 mesh. The experimental temperature is 77.3 k when the experimental adsorbate is liquid nitrogen, and 273.15 k when the experimental adsorbate is carbon dioxide. Before the experimental test, the appropriate amount of sample was weighed and put into a specific long tube (high-temperature and low-temperature resistance), and the vacuum degassing treatment was carried out at 150 °C for 4–6 h in order to remove the gas adsorbed on the surface of the material. After the degassing was complete, the sample was cooled to room temperature and fixed on the instrument to backfill helium and nitrogen (carbon dioxide) in turn. Then, the corresponding gas adsorption amount was determined by gradually changing the pressure at the test temperature, and the adsorption and desorption tests were carried out to obtain the adsorption–desorption isotherm curves of different samples.

## 3. Results

### *3.1. Mineral Composition Characteristics*

The overall performance of the Dawuba Formation in Well QSD-1 was dominated by carbonate minerals and clay minerals, followed by quartz minerals, and by fewer iron and magnesium minerals. The carbonate rock content was 4–93%, average 53%; the clay mineral content was 5–82%, average 33%; the quartz mineral content was 4–27%, average 11%; some samples contained iron–magnesium minerals and plagioclase: the pyrite content was 1–3%, average 2%, and the plagioclase content was 1–3%, average 1%.

Vertically, the fourth and third members of the Dawuba Formation are dominated by carbonate minerals (58–93%, average 70%), clay minerals (6–15%, average 10%) and felsic minerals (6–11%, average 7%). Carbonate minerals (32–61%, average 49%) and clay minerals (37–48%, average 40%) are the main minerals in the second member of the Dawuba Formation, followed by felsic minerals (average 8%) and iron–magnesium minerals (average 3%). The first member of the Dawuba Formation is dominated by clay minerals (54–82%, average 69%), followed by felsic minerals (16–33%, average 27%), and carbonate minerals (4–13%, average 6%) (Figure 3).

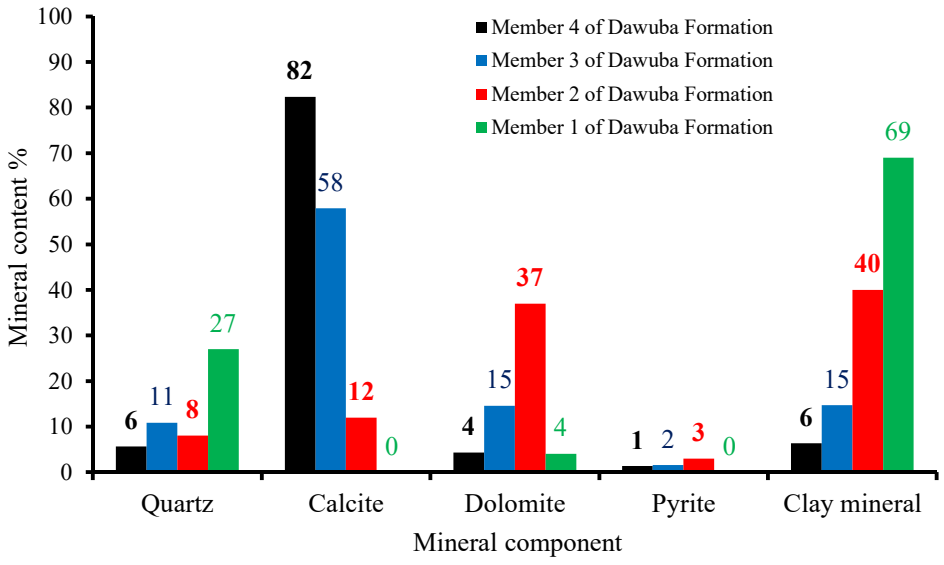


**Figure 3.** Mineral component content of the Dawuba Formation in Well QSD-1.

### 3.2. Pore Types and Morphological Characteristics

The SEM observation results show that several pore types are mainly observed in the Dawuba Formation of Well QSD-1: primary intergranular pore, organic matter pore, dissolved pore and intergranular pore of carbonate minerals, diagenetic fracture and interlayer pore fracture of clay minerals (Figure 4). It was found that the internal/intergranular pores of inorganic minerals such as clay minerals, quartz and feldspar, and the internal and marginal pores of organic matter differ greatly in size and morphology. The SEM observation shows that the distribution of different organic matter is quite different, and most of them are distributed in the shale matrix independently in the form of lumps and ribbons. Some organic matter grows together with the surrounding matrix minerals, filling in inorganic mineral particles (crystals) such as siliceous minerals, clay minerals or pyrite, and their boundaries are mostly mixed with the boundary between the mineral particles/crystals. There are a certain number of pores in the internal and edge of the organic matter, with large morphological differences. Ellipsoid, needle-like or irregular shapes are distributed, and the pore scale is relatively small. The content of the clay minerals in the samples is relatively high, and the pores in the crystal (grain) are most developed in the illite and illite–montmorillonite mixed layer. The intergranular pores of the clay minerals mostly exist in the natural faults between the laminated structures, particles and the internal plates of the particles. The bending lamellar pore aggregates are developed in the mineral crystals such as the illite and illite–montmorillonite mixed layer. Due to compaction, some clay minerals show a flake shape, and there are a large number of flat or linear pores between these flake clay minerals [28]. Compared with organic matter pores, the microfractures and clay mineral interlayer pore fractures in the Dawuba Formation shale are more developed, providing a good reservoir space for hydrocarbon gas occurrence [29].

### 3.3. Experimental Curve of Mercury Injection

It can be seen that the shape of the mercury injection–withdrawal curve of the samples in each member of the Dawuba Formation is quite different. The "hysteresis loop" formed by the inconsistency of the mercury injection curve and the mercury withdrawal curve is also the performance of the distribution of parameters such as the shape and connectivity of the reservoir space in the samples [30], reflecting the different characteristics of the strata in each member of the Dawuba Formation. The mercury withdrawal efficiency reflects the capillary effect recovery of the non-wetting phase, which indicates that the throat volume accounts for the percentage of the total volume of pores and throats in the core [31]. The larger the mercury withdrawal efficiency, the more uniform the size distribution of the pores and throats in the core. The maximum mercury saturation reflects the connectivity of the pore-fracture system and the degree of pore development.

The mercury injection test results show that there are macropores in the first, second and third members of the Dawuba Formation, the macropores in the second and third members are more developed than those in the first member and the pore connectivity is better in the first member. The pores in the first member are relatively developed and the pore size distribution is more uniform (Figure 5a).

The first member of the Dawuba Formation: when the pressure increases to about 10 MPa, the mercury curve shows a slow increasing trend, the pore sorting is relatively good and the pore size distribution is relatively uniform. The hysteresis loop of the mercury injection and withdrawal is wide, the volume difference of mercury injection and withdrawal is small and the efficiency of the mercury injection and withdrawal is relatively low, indicating that the corresponding throat is thin and the connectivity is poor in the mercury injection test range.

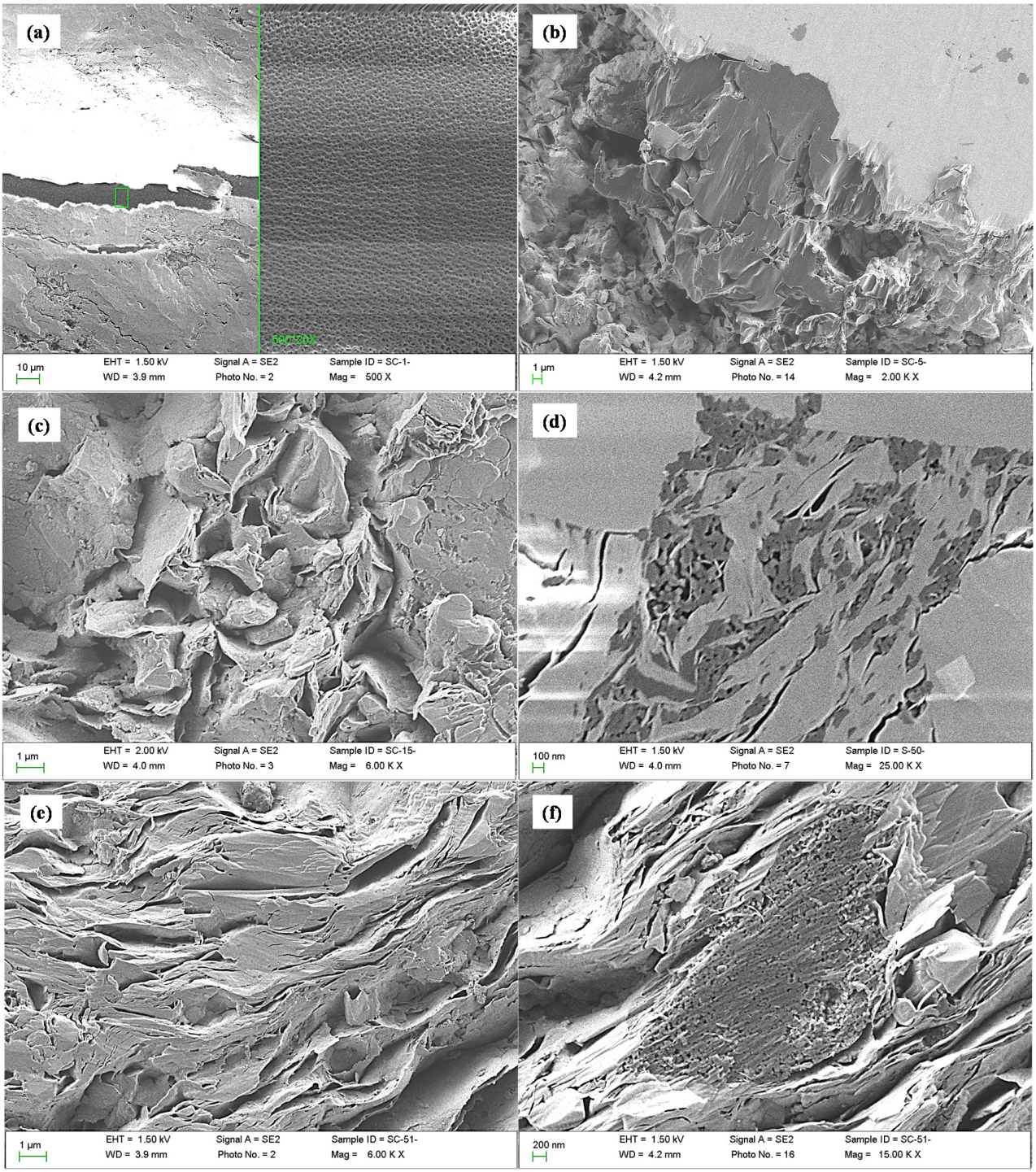


**Figure 4.** Microscopic characteristics of shale pores in the Dawuba Formation of Well QSD-1. (**a**) Black shale, member 4 of the Dawuba Formation, 1490 m, banded organic matter developed, micropores developed inside; (**b**) black shale, member 3 of the Dawuba Formation, 1531 m, organic matter is distributed in mineral grains, pores are developed in its interior and edge and some pores are connected to each other; (**c**) black shale, member 3 of the Dawuba Formation, 1660 m, clay mineral intergranular pore development; (**d**) black shale, member 2 of the Dawuba Formation, 1930 m, mixed distribution of organic matter and clay minerals; (**e**) black shale, member 1 of the Dawuba Formation, 1940 m, clay mineral interlayer fractures developed in a narrow strip; (**f**) black shale, member 1 of the Dawuba Formation, 1940 m, clay mineral interlayer fractures and micropores developed.

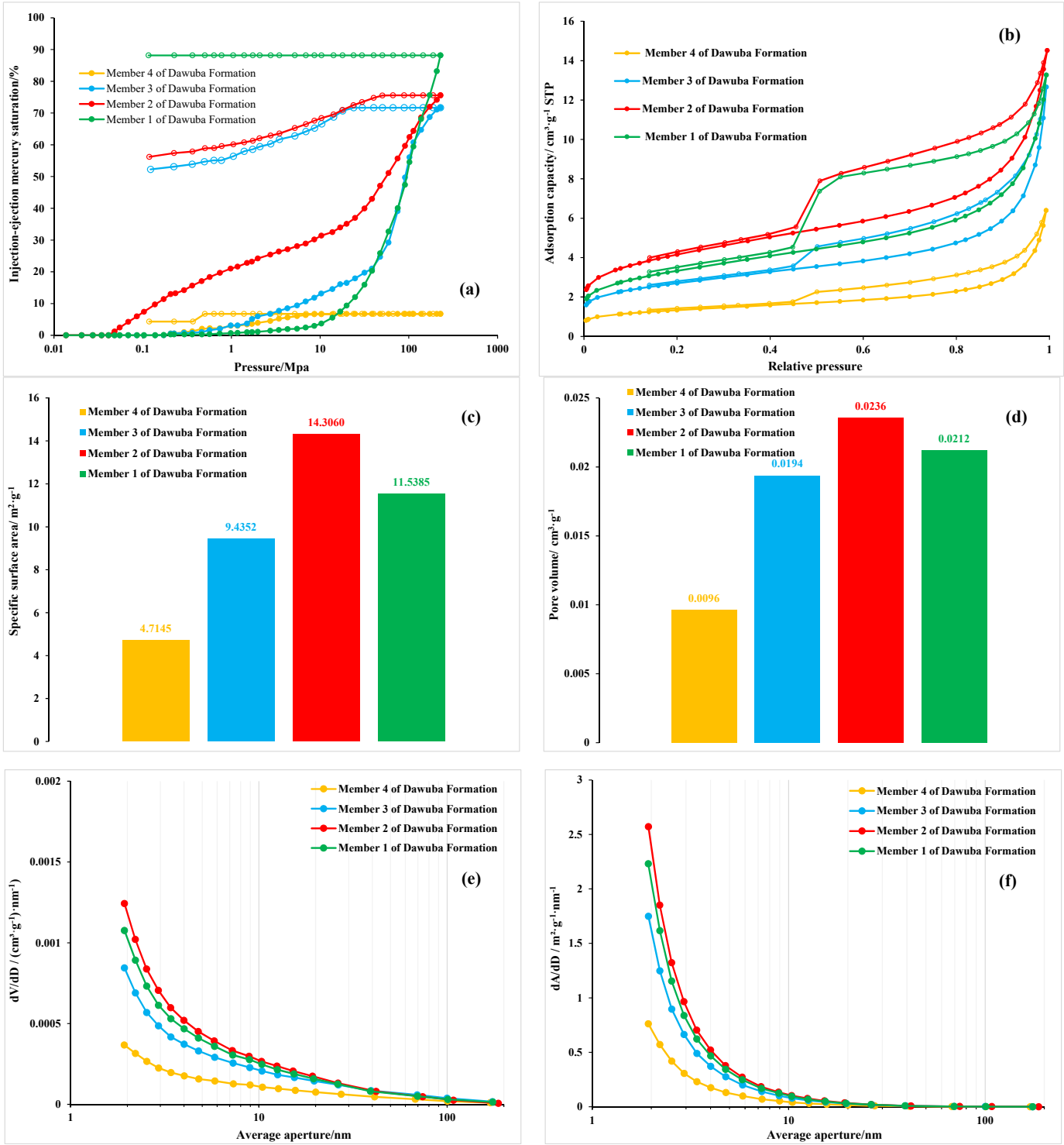


**Figure 5.** Pore distribution characteristics at different scales of the Dawuba Formation shale in Well QSD-1. (**a**) The mercury injection–withdrawal curve of each member of the Dawuba Formation shale; (**b**) nitrogen adsorption–desorption curve of shale in each member of the Dawuba Formation; (**c**) Based on the distribution of specific surface area of shale in each member of Dawuba Formation by $N_2$ adsorption; (**d**) shale pore volume distribution based on $N_2$ adsorption; (**e**) shale pore volume change rate distribution based on $N_2$ adsorption; (**f**) specific surface area distribution of shale in each member of the Dawuba Formation based on $N_2$ adsorption.

The second member of the Dawuba Formation: with the increase of pressure, the mercury injection curve showed a slow ladder increase trend; the sorting coefficient is about 4.45 and the displacement pressure is small. The corresponding maximum pore throat radius is 15.65 μm, and the maximum mercury saturation of the sample is 75%. The hysteresis loop of the mercury injection and withdrawal is wide and the volume difference between the mercury injection and withdrawal is large. The mercury withdrawal efficiency is about 25%, indicating that the macropores and mesopores of the sample are relatively developed in the pressure test range, and the pore connectivity is good.

The third member of Dawuba Formation: with the increase of pressure, the mercury curve shows a certain increasing trend. When the pressure increases to about 30 MPa, the mercury curve shows a ladder increasing trend. The sorting coefficient is about 4.21, the displacement pressure is 0.172 MPa and the maximum pore throat radius is 4.268 μm. It can be seen that the macropores of the third member samples are less developed than those of the second member samples. The maximum mercury saturation of the sample is about 70%, and the hysteresis loop of the mercury injection and withdrawal is wide. The volume difference of the mercury injection and withdrawal is large, and the mercury withdrawal efficiency is about 27%, indicating that the pore connectivity is good within the pressure test range.

The fourth member of Dawuba Formation: with the increase of pressure, the mercury injection curve exhibits little change. When the pressure increases to 400 MPa, the mercury saturation is less than 10%, indicating that the pores in the sample are relatively undeveloped.

### *3.4. Experimental Curve of $N_2$ and $CO_2$ Adsorption at Low Temperature*

Under the condition of low temperature (77 K), the $N_2$ adsorption–desorption curve can reflect the pore morphology. According to the four types of pores summarized by IUPAC [31], the main types of pores in the third and fourth members of the Dawuba Formation are close to the H3 type, that is, the open slit pores on four sides, while the main types of pores in the first and second members of the Dawuba Formation are close to the mixture of H1 and H2 types, indicating that the shales in the first and second members of the Dawuba Formation are mainly composed of regular tubular pores with openings at both ends and ink bottle-shaped pores with wide, thin necks (Figure 5b).

Based on the $N_2$ adsorption curve, the BJH adsorption model was used to calculate the pore volume and specific surface area of the shale samples in different layers (Figure 5c,d). The calculation results show that the pore volume and specific surface area of the second member of the Dawuba Formation are the largest, which are 14.3060 $m^2/g$ and 0.0236 $cm^3/g$, respectively, followed by the first, third and fourth members. It can be seen from the analysis of the change rates of the pore volume and specific surface area with pore size (Figure 5e,f) that with the increase of pore size, the change rate of the pore volume gradually decreases, indicating that the pore volume mainly changes significantly in the pores within the range of 2 nm to 5 nm. The specific surface area also shows a similar rule with the pore volume, indicating that the pore volume and specific surface area of the mesopore are mainly provided by the pores with pore size (2 nm–5 nm), and the contribution of a large pore size (5 nm–100 nm) to the pore volume and specific surface area is low.

## 4. Discussion

### *4.1. Distribution Characteristics of Total Pore Size of Shale*

Based on the experiments of high-pressure mercury injection and low-temperature gas adsorption ($N_2$ and $CO_2$), the pore distribution characteristics of shale from the nano scale to the micron scale were obtained [32]. Different experimental data have different characterization ranges and accuracy for pores. Micropores are mainly characterized by $CO_2$ adsorption data, mesopores are characterized by $N_2$ adsorption data and macropores

are characterized by high-pressure mercury injection data [33]. Thus, the full-aperture distribution characteristics of shale in each member of the Dawuba Formation are obtained.

It can be seen from the comparison that the pore volume of the shale pores in the Dawuba Formation in the study area is relatively developed in the mesopores and macropores, followed by the micropores. Among them, the shale pore characteristics of each member of the Dawuba Formation are similar, and the shale pore volume is dominated by medium pores (pore volume ratio > 50%), followed by macropores and micropores. The change of pore volume has three relatively stable peaks, which are 0.4 nm~0.6 nm, 5.6 nm~9.6 nm and 32.8 nm~500 nm (Figure 6, Table 2). The mesopores and macropores contribute about 89.78% of the pore volume, and the micropores contribute about 10.22% of the pore volume (Table 2).

The distribution of the dV/dD pore volume and pore size in the full pore size range of the shale samples in each member of the Dawuba Formation shows that the pores of the samples are mainly distributed in the micropore members and some mesopore members, among which the number of mesopores with a pore size of about 10 nm in the first and third members is more than that in the second and fourth members (Figure 7).

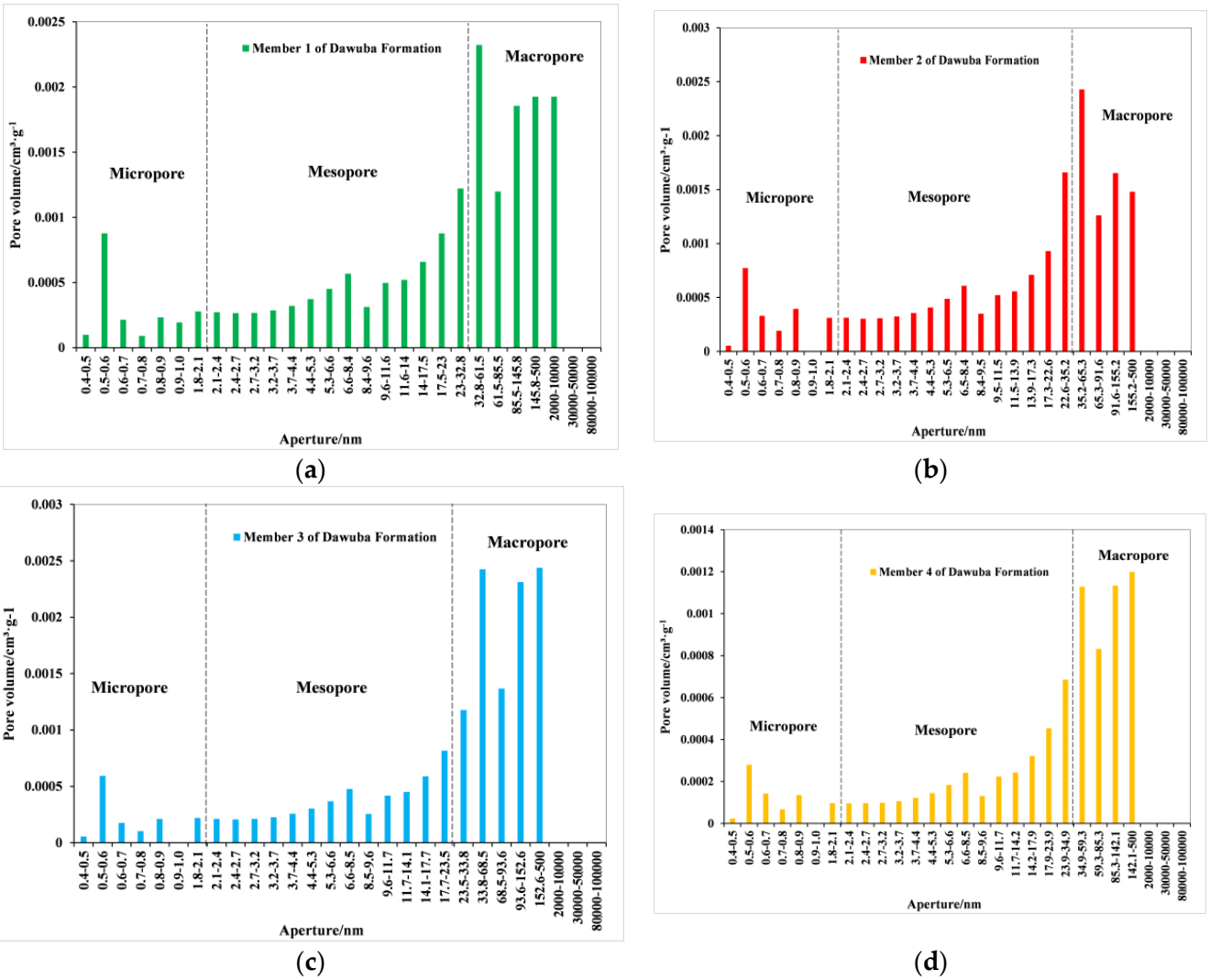


**Figure 6.** Whole pore size distribution of shale pore volume of the Dawuba Formation in the Qianxi area. (**a**) Member 1 of the Dawuba Formation; (**b**) member 2 of the Dawuba Formation; (**c**) member 3 of the Dawuba Formation; (**d**) member 4 of the Dawuba Formation.

**Table 2.** Statistics of shale pore volume of the Dawuba Formation in the Qianxi area.

| Samples | Pore Volume/($cm^3 \cdot g^{-1}$) | | | | Pore Volume Ratio/% | | |
|---|---|---|---|---|---|---|---|
| | Micropore | Mesopore | Macropore | Total Pore Volume | Micropore | Mesopore | Macropore |
| Member 1 of Dawuba | 0.001985 | 0.009215 | 0.006907 | 0.018107 | 10.96 | 50.89 | 38.15 |
| Member 2 of Dawuba | 0.002052 | 0.01026 | 0.004396 | 0.016708 | 12.28 | 61.41 | 26.31 |
| Member 3 of Dawuba | 0.001358 | 0.008392 | 0.006118 | 0.015868 | 8.56 | 52.89 | 38.56 |
| Member 4 of Dawuba | 0.000745 | 0.004276 | 0.003165 | 0.008186 | 9.10 | 52.24 | 38.66 |
| Average value | 0.001535 | 0.008036 | 0.0051465 | 0.014717 | 10.22 | 54.36 | 35.42 |

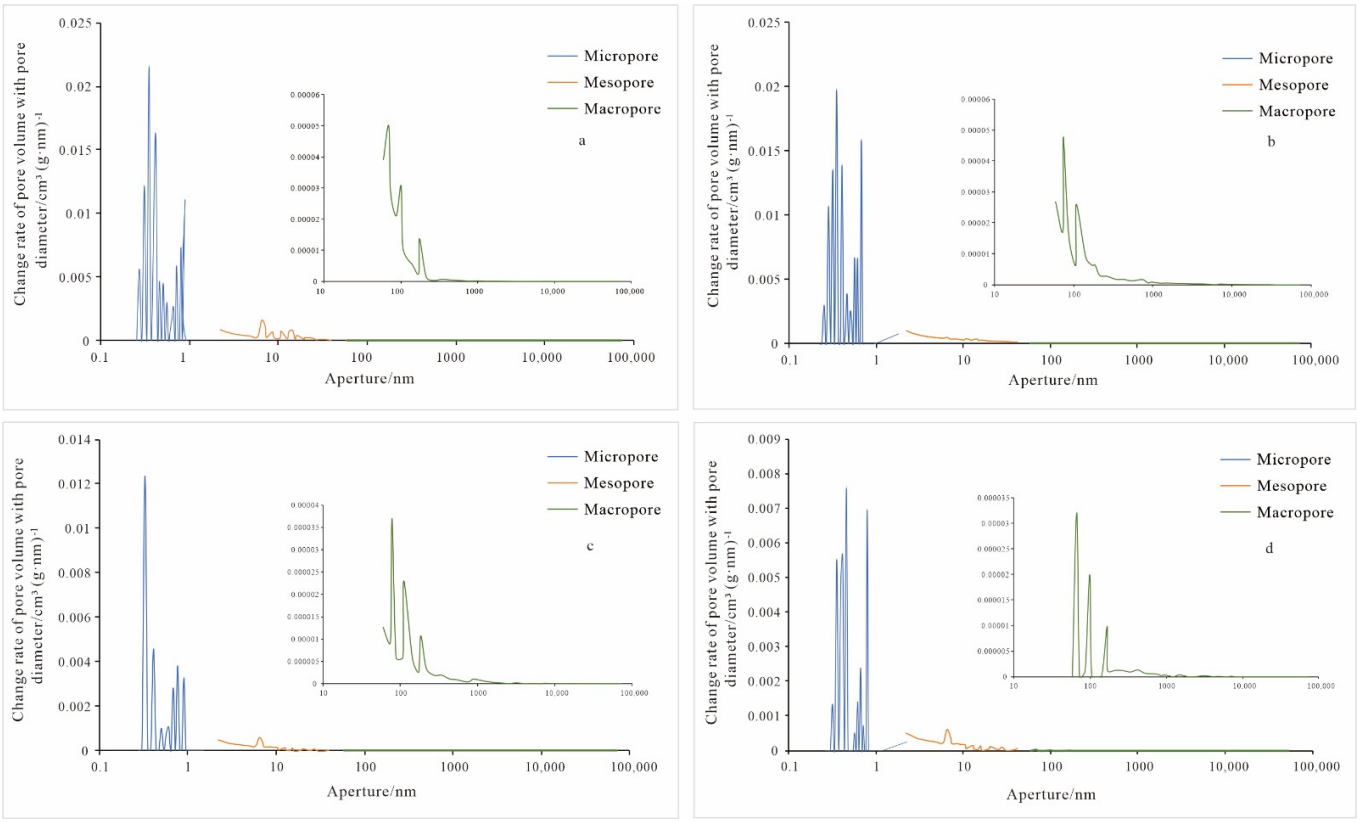


**Figure 7.** Variation rate curve of total pore volume with pore diameter of Dawuba Formation shale in the Qianxi area. (**a**) Member 1 of the Dawuba Formation; (**b**) member 2 of the Dawuba Formation; (**c**) member 3 of the Dawuba Formation; (**d**) member 4 of the Dawuba Formation.

From the analysis of the specific surface area provided by the shale pores, the specific surface area of the shale pores in the Dawuba Formation in the study area is mainly provided by micropores and mesopores. Pores contribute 93% of the specific surface area of the shale in the Dawuba Formation, and pores less than 0.6 nm in each member are the main contributors to the specific surface area. With the increase of pore diameter, the specific surface area shows a downward trend; the specific surface area provided by the mesopores is generally less than 0.5 $m^2/g$, and the specific surface area provided by the macropores is one order of magnitude smaller than that of the mesopores (Figure 8, Table 3).

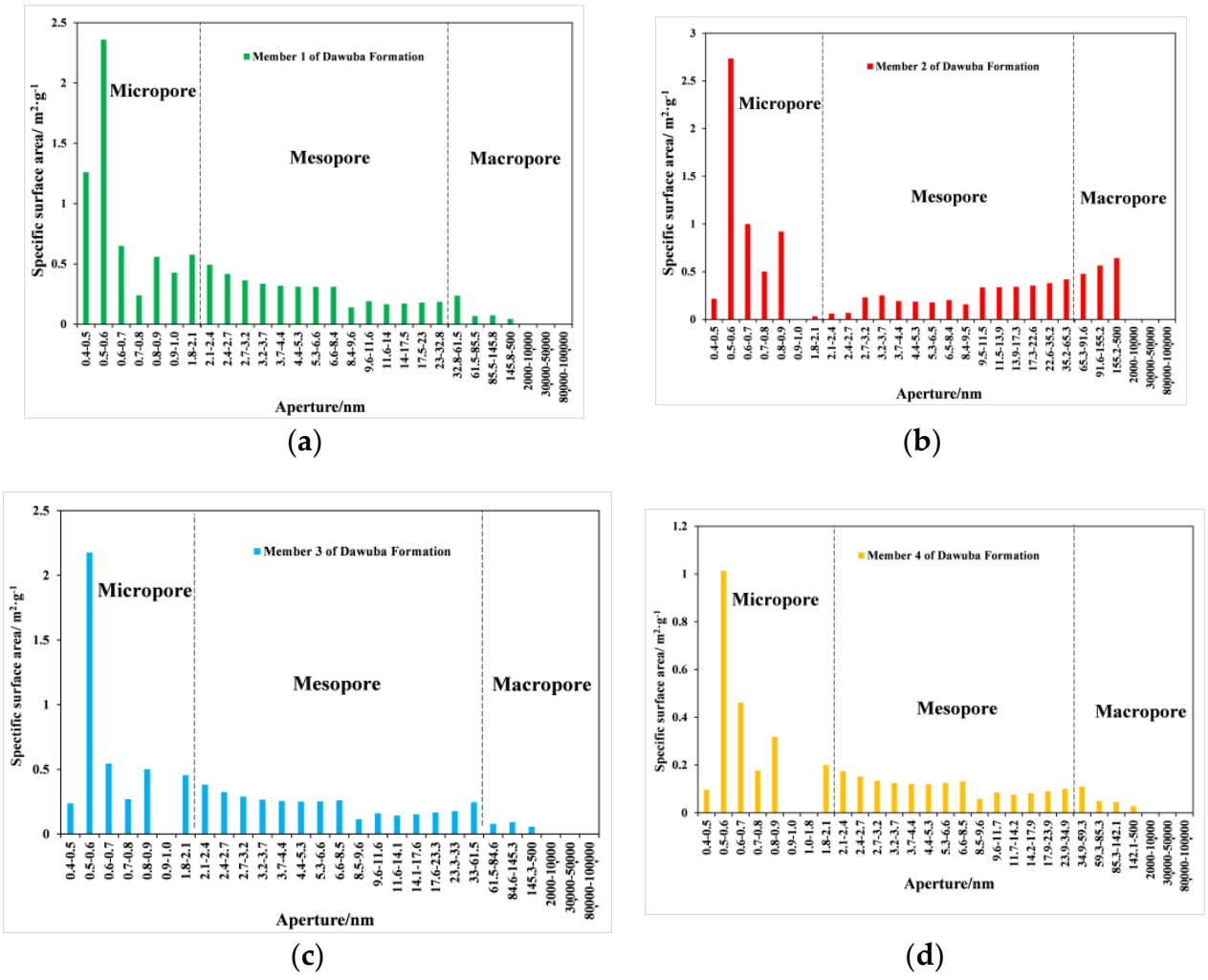


**Figure 8.** Distribution of specific surface area and full aperture of Dawuba Formation shale in the Qianxi area. (**a**) Member 1 of the Dawuba Formation; (**b**) member 2 of the Dawuba Formation; (**c**) member 3 of the Dawuba Formation; (**d**) member 4 of the Dawuba Formation.

**Table 3.** Statistics of specific surface area of Dawuba Formation shale in the Qianxi area.

| Samples | Pore Volume/($cm^3 \cdot g^{-1}$) | | | | Pore Volume Ratio/% | | |
|---|---|---|---|---|---|---|---|
| | Micropore | Mesopore | Macropore | Total Pore Volume | Micropore | Mesopore | Macropore |
| Member 1 of Dawuba | 0.001985 | 0.009215 | 0.006907 | 0.018107 | 10.96 | 50.89 | 38.15 |
| Member 2 of Dawuba | 0.002052 | 0.01026 | 0.004396 | 0.016708 | 12.28 | 61.41 | 26.31 |
| Member 3 of Dawuba | 0.001358 | 0.008392 | 0.006118 | 0.015868 | 8.56 | 52.89 | 38.56 |
| Member 4 of Dawuba | 0.000745 | 0.004276 | 0.003165 | 0.008186 | 9.10 | 52.24 | 38.66 |
| Average value | 0.001535 | 0.008036 | 0.0051465 | 0.014717 | 10.22 | 54.36 | 35.42 |

### *4.2. Discussion on Shale Pore Control*

The development of nanopores in shale may be affected by many factors [34]. Based on the analysis of the relationship between pore-specific surface area, pore volume and total organic carbon (TOC), it is considered that TOC has a good positive correlation with the development of pores in shale. The specific surface area of shale micropores has the

best correlation with TOC. As TOC increases from 0.53% to 1.22%, the specific surface area of the micropores increases from 1.03 $m^2/g$ to 6.07 $m^2/g$, and the correlation coefficient is 0.88 (Figure 9a). The correlation between mesopore-specific surface area and TOC is 0.61, and the correlation between the macropore-specific surface area and TOC is poor. The relationship between pore volume and the TOC of shale is similar to that of the specific surface area. The pore volume of the micropores and mesopores has good correlation with TOC, followed by macropores (Figure 9b). It indicates that the organic matter contributes more to the micropores, which was also observed from all of the densely packed organic matter pores in Figure 4.

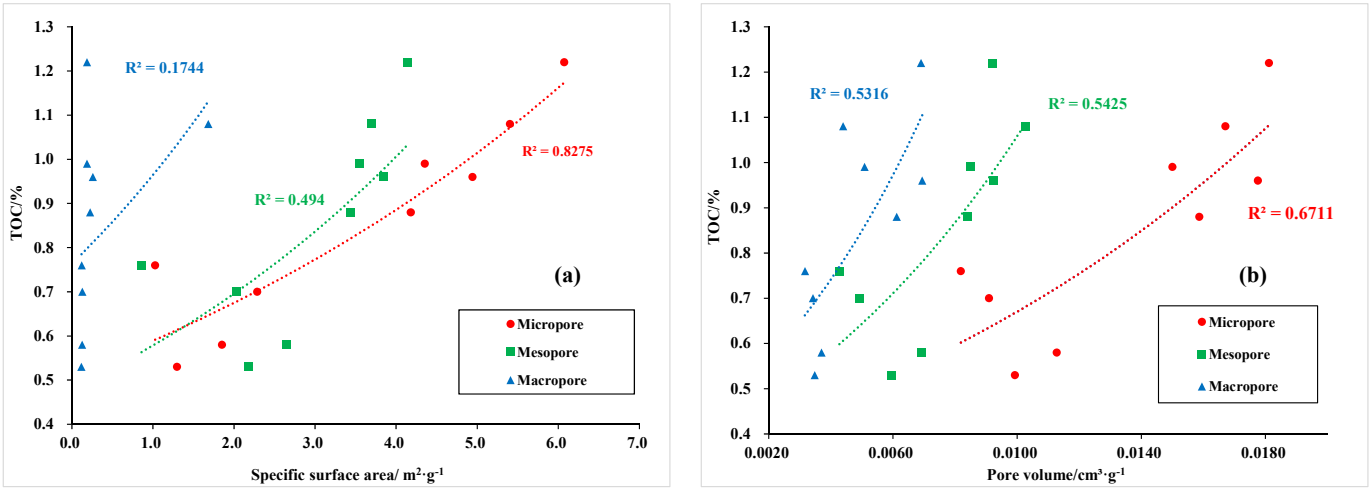


**Figure 9.** Relationship between pore-specific surface area, pore volume and TOC of Dawuba Formation shale in the Qianxi area. (**a**) Relationship between pore-specific surface area and TOC; (**b**) Relationship between pore volume and TOC.

Through the comparison of the shale mineral content and pore characteristics, it is found that there is a certain correlation between shale pores and mineral content in different pore size ranges [35]. The specific surface area and pore volume show a positive correlation with quartz and clay minerals, but a negative correlation with carbonate minerals. In view of the highest correlation coefficient, the correlation between clay mineral content and pore-specific surface area and pore volume is the best regardless of pore size (micropore, mesopores or macropores), followed by carbonate minerals and quartz mineral content, indicating little effect on pore development and specific surface area (Figure 10). For pores of different size ranges, the clay mineral content is positively correlated with the specific surface area of micropores and mesopores, and the correlation coefficient is more than 0.8 (Figure 10e). The clay mineral content has a good correlation with the micropore and mesopore volume of the sample (Figure 10f). Quartz minerals contribute greatly to the pore volume of macropores (Figure 10b). In shale reservoirs, quartz acts more likely as a rock framework, with clay minerals as interstitial materials. Hence, clay minerals have a stronger impact on pores of small sizes. In addition, due to the strong chemical cementation of carbonate minerals, the development of nano–micropores will be inhibited to varying degrees. In addition, the pores between carbonate particles are easily cemented and filled by clay minerals and organic matter, so the content of carbonate minerals is negatively correlated with the pore volume and specific surface area (Figure 10c,d).

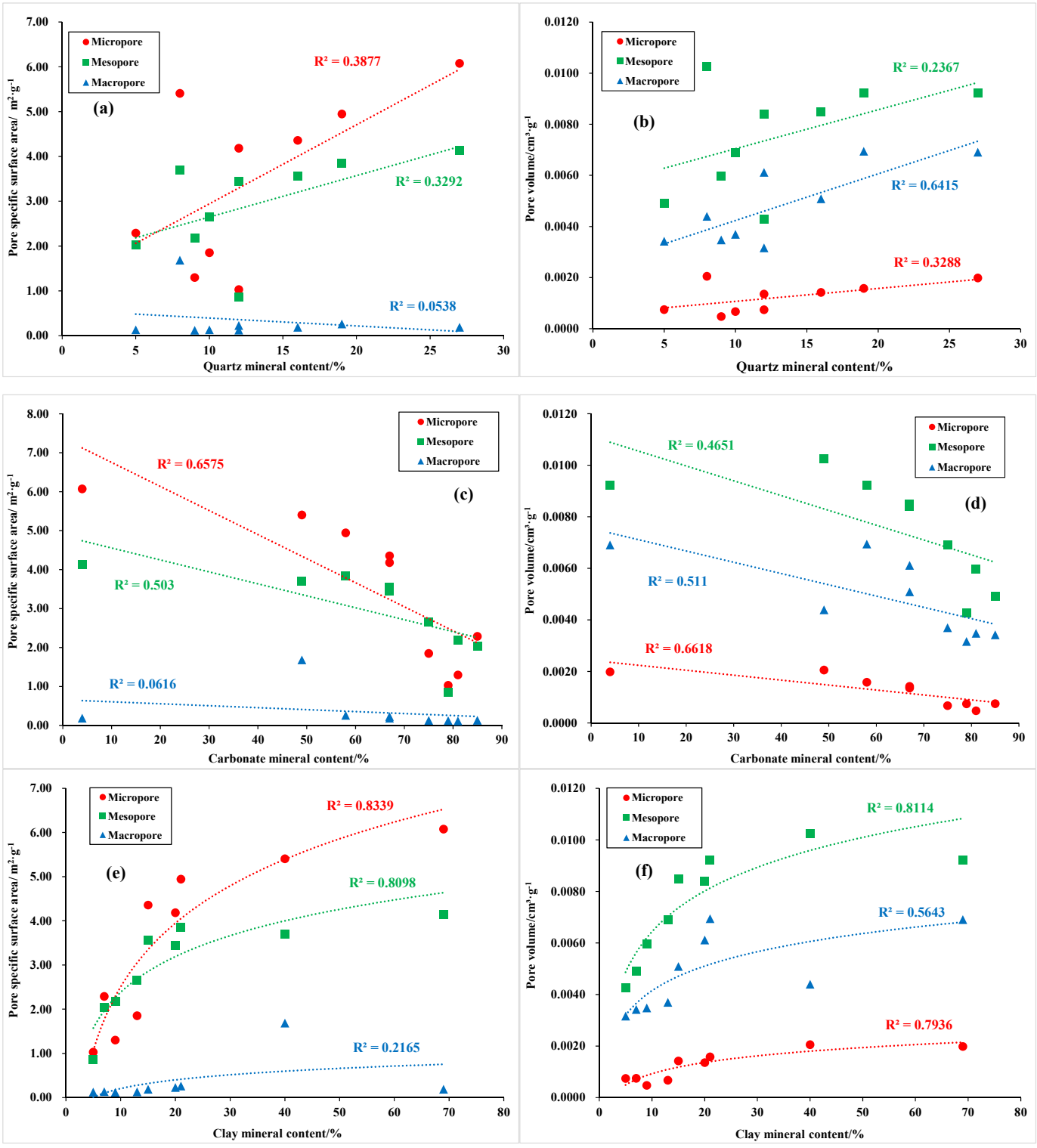


**Figure 10.** Relationship between pore-specific surface area, pore volume and quartz, carbonate and clay minerals of shale in the Qianxi area. (**a**) Relationship between pore-specific surface area and Quartz mineral content; (**b**) Relationship between pore volume and Quartz mineral content; (**c**) Relationship between pore-specific surface area and Carbonate mineral content; (**d**) Relationship between pore volume and Carbonate mineral content; (**e**) Relationship between pore-specific surface area and Clay mineral content; (**f**) Relationship between pore volume and Clay mineral content.

The analysis shows that the organic carbon content and clay mineral content of the Carboniferous Dawuba Formation in the Qianxi area are the main controlling factors for the specific surface areas of micropores and mesopores, and carbonate minerals and quartz minerals are positively correlated with the macropore volume of the samples. The analysis shows that the TOC and mineral components, to some extent, mainly affect the adsorption capacity of shale by affecting its specific surface area and pore volume and other pore structures. The porosity of organic matter makes it form a huge internal surface area. Due to the development of a layered structure, clay minerals also have large specific surface area and micropore volume. The specific surface area of organic matter pores and pores between clay minerals plays a major role in the specific surface area of the sample, which can provide more adsorption points for methane adsorption and is the main factor affecting the adsorption capacity of the sample. In the process of diagenetic evolution, brittle minerals such as quartz and carbonate play a supporting and protecting role in intergranular organic matter, intergranular pores and interlayer fractures, and play a decisive role in the enrichment of free gas in shale.

The intersection analysis of the clay mineral content of the samples with the total hydrocarbon values at the locations shows that the high total hydrocarbon values rise at the sites with a high clay content (Figure 11). It indicates that the shale gas is fully enriched and effectively preserved at the high clay sites. In addition, the comparison of total hydrocarbon with the specific surface area and pore volume shows that the gas is mainly adsorbed on the micropores and mesopores with a larger specific surface area, and is mainly enriched in the pore volume provided by the micropores. Combining the SEM and FMI results, it is concluded that clay minerals—especially those with microfractures and interlayer joints—are the main storage space for shale gas in the Dawuba Formation.

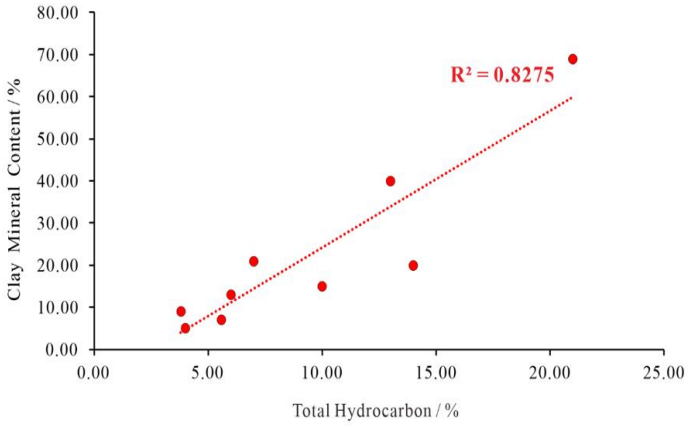


(**a**)

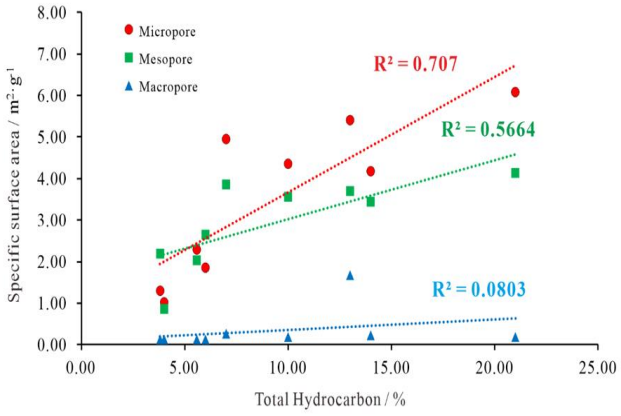


(**b**)

**Figure 11.** *Cont*.

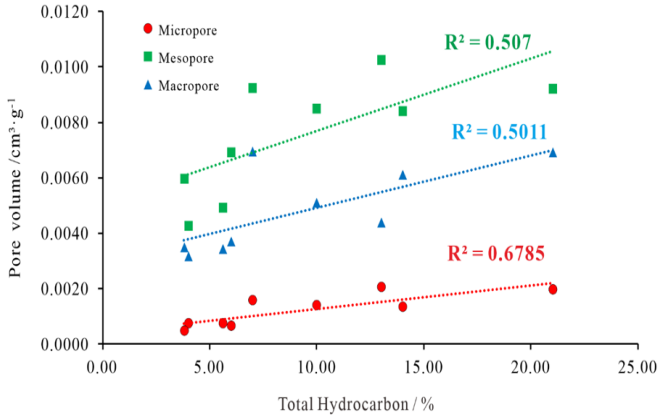


(**c**)

**Figure 11.** Cross plot of total hydrocarbon, clay minerals, specific surface area and pore volume. (**a**) Relationship between Clay mineral content and Total Hydrocarbon; (**b**) Relationship between pore-specific surface area and Total Hydrocarbon; (**c**) Relationship between pore volume and Total Hydrocarbon.

## 5. Conclusions

(1) The micropores and mesopores of Dawuba Formation shale in the Qianxi area are relatively developed, followed by macropores. In terms of pore volume, mesopores and macropores contribute about 89.78% of the pore volume, and micropores contribute about 10.22% of the pore volume. In terms of the specific surface area, micropores and mesopores contribute 93% of the specific surface area of Dawuba Formation shale, and pores less than 0.6 nm are the main contributors.

(2) There are many types of pores in the shale of the Dawuba Formation. However, compared with organic pores, the gas-bearing properties are better in the parts of the shale of the Dawuba Formation where clay minerals are developed, and not only are the specific surface area and pore volume of the micropores and mesopores larger in these parts, but also have more developed microfractures and interlayer pore fractures of clay minerals, providing a good reservoir space for the occurrence of hydrocarbon gases.

(3) The pore development characteristics of the different members in the Dawuba Formation are different. The first and second members of the Dawuba Formation are mainly regular tubular pores with open ends and ink bottle-like pores, which are thin-necked and wide-bodied, with the pore volume mainly provided by pores above 2 nm, followed by micropores. The specific surface area mainly provided by pores below 2 nm, and pores above 50 nm in the second section, also contribute a certain amount of specific surface area. Due to the high clay content, the first and second members of the Dawuba Formation have more pores. Due to the high clay content, more microfractures and interlayer pore fractures are developed in the first and second members. The third and fourth members of the Dawuba Formation are mainly slit-like pores, which are open on four sides. More than 90% of the pore volume comes from pores above 2 nm and more than 80% of the specific surface area comes from pores below 10 nm.

(4) The organic carbon content and clay mineral content of shale affect the adsorption capacity of shale by affecting its pore structure, such as the specific surface area and pore volume, which are the main control factors of the shale adsorption capacity of the Dawuba Formation in the Qianxi area. The organic carbon content of the shale here has a good correlation with the specific surface area and pore volume of the micropores. The clay mineral intergranular pores play a major role in the specific surface area of the mesopores and macropores.

**Author Contributions:** Conceptualization, K.Y. and W.H.; methodology, Q.C.; software, X.F.; validation, S.L., C.J. and T.W.; formal analysis, T.L. and C.W.; investigation, T.L. and K.Y.; resources, K.Y.; data curation, T.L. and X.C.; writing—original draft preparation, K.Y.; writing—review and editing, K.Y.; visualization, X.F.; supervision, W.H.; project administration, K.Y.; funding acquisition, K.Y. and S.L. All authors have read and agreed to the published version of the manuscript.

**Funding:** This research was funded by the China Geological Survey Projects "Geological survey of shale gas in Guizhong-Nanpanjiang area"(grant no.DD20190088).

**Institutional Review Board Statement:** Not applicable.

**Informed Consent Statement:** Informed consent was obtained from all subjects involved in the study.

**Data Availability Statement:** The data has been included in the manuscript.

**Conflicts of Interest:** The authors declare no conflict of interest.

## References

1. Dong, D.; Zou, C.; Dai, J.; Huang, S.; Zheng, J.; Gong, J.; Qiu, Z. Suggestions on the development strategy of shale gas in China. *Nat. Gas Geosci.* **2016**, *27*, 397–406. [CrossRef]
2. Jia, C.Z.; Pang, X.Q.; Jiang, F.J. Research status and development directions of hydrocarbon resources in China. *Pet. Sci. Bull.* **2016**, *1*, 2–23.
3. Zou, C.; Zhao, Q.; Cong, L.; Wang, H.; Shi, Z.; Wu, J.; Pan, S. Development progress, potential and prospect of shale gas in China. *Nat. Gas Ind.* **2021**, *41*, 1–14.
4. Liu, G.; Liu, B.; Huang, Z.; Chen, Z.; Jiang, Z.; Guo, X.; Chen, L. Hydrocarbon distribution pattern and logging identification in lacustrine fine-grained sedimentary rocks of the Permian Lucaogou formation from the Santanghu basin. *Fuel* **2018**, *222*, 207–231. [CrossRef]
5. Liu, G.; Zhai, G.; Zou, C.; Cheng, L.; Guo, X.; Xia, X.; Zhou, Z. A comparative discussion of the evidence for biogenic silica in Wufeng-Longmaxi siliceous shale reservoir in the Sichuan basin, China. *Mar. Pet. Geol.* **2019**, *109*, 70–87. [CrossRef]
6. Liu, G.; Zhai, G.; Huang, Z.; Zou, C.; Xia, X.; Shi, D.; Zhang, S. The effect of tuffaceous material on characteristics of different lithofacies: A case study on Lucaogou Formation fine-grained sedimentary rocks in Santanghu Basin. *J. Pet. Sci. Eng.* **2019**, *179*, 355–377. [CrossRef]
7. Liu, G.; Huang, Z.; Jiang, Z.; Chen, J.; Chen, F.; Xing, J. Gas adsorption capacity calculation limitation due to methane adsorption in low thermal maturity shale: A case study from the Yanchang Formation, Ordos Basin. *J. Nat. Gas Sci. Eng.* **2016**, *30*, 106–118. [CrossRef]
8. Liu, G.; Huang, Z.; Chen, F.; Jiang, Z.; Gao, X.; Li, T.; Han, W. Reservoir characterization of Chang 7 member shale: A case study of lacustrine shale in Yanchang Formation, Ordos Basin, China. *J. Nat. Gas Sci. Eng.* **2016**, *34*, 458–471. [CrossRef]
9. Liu, G.; Zhai, G.; Zou, C.; Huang, Z.; Liu, B.; Guo, X.; Wang, H. Amorphous silica and its effects on shale reservoir: A case study about Yanchang formation lacustrine shale, Ordos Basin. *Energy Sources Part A Recovery Util. Environ. Eff.* **2018**, *41*, 975–989. [CrossRef]
10. Yuan, K.; Huang, W.; Fang, X.; Wang, T.; Lin, T.; Chen, R. Evaluation of Favorable Shale Gas Intervals in Dawuba Formation of Ziyun Area, South Qian Depression. *Geofluids* **2021**, *2021*, 6688141. [CrossRef]
11. Li, F.J.; Zheng, R.C.; Zhou, X.J.; Zhao, J.X.; Jiang, B. Late Palaeozoic tectonic evolution and basin prototype in southern China. *Sediment. Geol. Tethyan Geol.* **2009**, *29*, 93–99.
12. Li, S.W. The effect analyses and aspects of petroleum exploration in Yunnan-Guizhou-Guangxi region. *Oil Gas Geol.* **1985**, *6*, 221–225.
13. Chen, S.; Li, B.B.; Zhang, Y.; Wang, Z.H. Microscopic seepage mechanism of shale gas reservoir. *Sci. Sin Tech.* **2021**, *51*, 580–590. (In Chinese) [CrossRef]
14. Dong, D.Z.; Zou, C.N.; Li, J.Z.; Wang, S.J.; Li, X.J.; Wang, Y.M.; Huang, J.L. Resource potential, exploration and development prospect of shale gas in the whole world. *Geol. Bull. China* **2011**, *30*, 324–336.
15. Jia, C.Z.; Pang, X.Q.; Song, Y. The mechanism of unconventional hydrocarbon formation: Hydrocarbon self-containment and intermolecular forces. *Pet. Explor. Dev.* **2021**, *48*, 437–452. [CrossRef]
16. Jiang, Z.X.; Tang, X.L.; Li, Z.; Huang, H.X.; Yang, P.-P.; Yang, X.; Li, W.-B.; Hao, J. The whole-aperture pore structure characteristic and its effect on gas content of the Longmaxi Formation shale in the southeastern Sichuan basin. *Earth Sci. Front.* **2016**, *23*, 126–134.
17. Jiang, Y.; Dong, D.Z.; Qi, L.; Shen, Y.F.; Jiang, C.; He, F. Basic features and evaluation of shale gas reservoirs. *Nat. Gas Ind.* **2010**, *30*, 7–12.
18. Jia, B.; Xian, C.G. Permeability measurement of the fracture-matrix system with 3D embedded discrete fracture model. *Pet. Sci.* **2022**, *in press*. [CrossRef]
19. Mudunuru, M.K.; O'Malley, D.; Srinivasan, S.; Hyman, J.D.; Sweeney, M.R.; Frash, L.; Viswanathan, H.S. Physics-Informed Machine Learning for Real-time Reservoir Management. In Proceedings of the AAAI Spring Symposium: MLPS, Palo Alto, CA, USA, 23–25 March 2020.

20. Srinivasan, S.; O'Malley, D.; Mudunuru, M.K.; Sweeney, M.R.; Hyman, J.D.; Karra, S.; Viswanathan, H.S. A machine learning framework for rapid forecasting and history matching in unconventional reservoirs. *Sci. Rep.* **2021**, *11*, 1–15. [CrossRef]
21. Liu, F.; Huang, Y.Y. Research on Pore Structure of Shale Based on High Pressure Mercury Injection, Nitrogen Adsorption and Carbon Dioxide Adsorption. *China Coalbed Methane* **2021**, *18*, 8–12.
22. Yuan, K.; Chen, R.; Lin, T.; Fang, X.; Qin, Y.; Wang, C.; Center, G.S. Petrological characteristics and sedimentary environment in the southern Guizhou during the Late Carboniferous. *Pet. Geol. Exp.* **2019**, *41*, 38–44.
23. Yuan, K.; Wang, C.; Qin, Y.; Yu, S.; Chen, R.; Shi, D.; Zhou, Z. The discovery of Carboniferous shale gas in Qianziye-1 well of Qianan (southern Guizhou) depression. *Geol. China* **2017**, *44*, 1253–1254, (In Chinese with English abstract).
24. Yuan, K.; Wang, K.; Gong, S.; Lu, S.; Fang, X. Shale Gas Enrichment Features and Impacting Factors in Carboniferous Dawuba Formation, Southern Guizhou Area. *Coal Geol. China* **2018**, *30*, 28–34.
25. Liu, G.; Zhai, G.; Yang, R.; He, T.; Wei, B. Quartz crystallinity index: New quantitative evidence for biogenic silica of the Late Ordovician to Early Silurian organic-rich shale in the Sichuan Basin and adjacent areas, China. *Sci. China Earth Sci.* **2021**, *64*, 773–787. [CrossRef]
26. Xie, X.Y.; Tang, H.M.; Wang, C.H.; Bai, R.; Wang, Z.L. Contrast of nitrogen adsorption method and mercury porosimetry method in analysis of shale's pore size distribution. *Nat. Gas Ind.* **2006**, *26*, 100–102. [CrossRef]
27. Tian, H.; Zhang, S.C.; Liu, S.B.; Zhang, H. Determination of organic-rich shale pore features by mercury injection and gas adsorption methods. *Acta Pet. Sin.* **2012**, *33*, 419–427.
28. Yang, Q.; Mao, Z.; Shao, M.R. Research methods and prospects of nanopore structure in shale gas reservoirs. *Energy Chem. Ind.* **2021**, *42*, 7–13.
29. Yu, B.S. Classification and characterization of gas shale pore system. *Earth Sci. Front.* **2013**, *20*, 211–220.
30. Ji, L.; Qiu, J.; Xia, Y.; Zhang, T. Micro-pore characteristics and methane adsorption properties of common clay minerals by electron microscope scanning. *Acta Pet. Sin.* **2012**, *33*, 249–256.
31. Nie, H.K.; Tang, X.; Bian, R.K. Controlling factors for shale gas accumulation and prediction of potential development area in shale gas reservoir of South China. *Acta Pet. Sin.* **2009**, *30*, 484–491.
32. Wang, Y.M.; Dong, D.Z.; Li, J.Z.; Wang, S.J.; Li, X.J.; Wang, L. Reservoir characteristics of shale gas in Longmaxi Formation of the Lower Silurian, southern Sichuan. *Acta Pet. Sin.* **2012**, *33*, 551–561.
33. Xie, Z.T.; Hu, H.Y.; Yuan, H.P.; Liu, J.P.; Wang, T.; Liu, L.H. Influence of shale components on the pore development differences between wufeng-longmaxi formation and Niutitang formation: A Case Study of JY-1 Well in Southeast Chongqing and CY-1 Well in Northwest Hunan. *Geol. Resour.* **2021**, *30*, 143–152.
34. Yang, X.; Jiang, Z.X.; Song, Y.; Huang, H.X.; Tang, X.L.; Ji, W.M. A Comparative Study on Whole-aperture Pore Structure Characteristics between Niutitang and Longmaxi Formation of High-matruity Marine Shales in Southeastern Chongqingelt. *Geol. J. China Univ.* **2016**, *22*, 368–377.
35. Yuan, K.; Fang, X.X.; Lin, T.; Bao, S.J.; Shi, D.S.; Zhang, C. Geochemical features and sedimentary conditions of Middle-Devonian shale in the northwestern central Guangxi depression. *Geol. Explor.* **2017**, *53*, 179–186.